AC Side Impedance Modeling Method of Multi-level Converter Considering Complete Control Structure

Qunqiao Wang, Chongru Liu, Hanxing Lin
State Key Laboratory of Alternate Electrical Power System with Renewable Energy Sources
North China Electric Power University
Beijing, China
435438959@qq.com

2022 IEEE 5th International Electrical and Energy Conference (CIEEC) | 978-1-6654-1104-2/22/$31.00 ©2022 IEEE | DOI: 10.1109/CIEEC54735.2022.9846510

***Abstract*—Modular multilevel converter (MMC) based High Voltage Direct Current Transmission (HVDC) has been developing rapidly in the fields of wind new energy integration and AC grid asynchronous interconnection. The AC side impedance modeling of MMC is an important basis for analyzing the stability of MMC-HVDC system and its interconnection system. Firstly, the harmonic distribution in MMC is analyzed. Then based on the harmonic linearization principle, considering the current inner loop control, DC voltage outer loop control, power outer loop control and circulating current control, this paper proposes a building modular multilevel converter small signal impedance model method. Finally, the MMC simulation model is established in the PSCAD/EMTDC environment and the accuracy of the proposed model is verified and the influence of different control mode on impedance characteristics of MMC is analyzed.**

Keywords—Modular multilevel converter (MMC); flexible DC power transmission;harmonic linearization; impedance

I. INTRODUCTION

HVDC flexible technology has gradually been widely used in power transmission systems due to its advantages of high controllability, low harmonic content and flexible structure [1]-[3]. In recent years, with the increasing number of VSC-HVDC projects, the HVDC flexible technology based on MMC has become a hotspot of current research. Flexible DC power grid has the characteristics of nonlinear and strong coupling, so it is very easy to be affected by harmonics. When harmonics flow into DC power grid through MMC converter station, it may cause the oscillation of the whole transmission system [4]. At present, several MMC-HVDC projects in the run or test phase have occurred oscillation phenomenon: 1.6khz high-frequency oscillation occurred in the INELFE Networking project [5]. 30Hz synchronous oscillation occurred in Offshore Wind Energy Flexible Direct Current Transmission in South Australia [6]. High frequency oscillation of 1.2khz occurred in the Luxi VSC-HVDC Transmission Project [7]. 0.7khz and 1.8khz high-frequency oscillations occurred successively in Chongqing-Hubei HVDC Project [8]. The oscillation poses a great threat to the safe and stable operation of flexible DC power grid.

At present, the stability analysis methods of grid-connected MMC are mainly divided into state space method based on time domain and impedance method based on frequency domain. State space method is based on the MMC HVDC system in working point based on linearization, the mathematical model to get the state space model of the system, and through the analysis of the eigenvalues and eigenvectors of the state matrix to determine the stability of the system, but the order of small signal model is usually too high and not conducive to the stability analysis, which makes the whole process cumbersome and complex [9]-[10]. Impedance method is respectively dividing inverter and ac power grid as an independent subsystem, according to their respective characteristic respectively, and the stability of the system is analyzed by Nyquist criterion. The system stability analysis is simple and effective, compared with other analysis methods, for the characteristics of oscillation point accurately, It is suitable for stability analysis of complex VSC-HVDC system. Therefore, frequency domain analysis method based on impedance method has become a common method to analyze the stability of MMC-HVDC system at present [11], and the establishment of accurate MMC impedance model is the premise to analyze the stability of grid-connected system.

In [12], the AC/DC impedance model of MMC was derived based on the operation principle and continuous model of MMC. The equivalent impedance obtained was similar to RLC series circuit, and the test signal method was used for verification, but the error was large in the low-frequency range, and the model was not accurate enough. In [13], harmonic linearization method was adopted to establish the AC impedance model of MMC, and the internal circulation and capacitance voltage steady-state harmonics were taken into account. However, only the influence of circulating current controller was considered and other control links was not taken into account. [14] is proposed for the first time the concept of harmonic linearization, and apply the AC impedance MMC model is set up, but also considers the MMC all the electric parameters within the influence of high harmonics, but it ignores outer loop control, and asymmetric outer loop control such as DC voltage control and power control is one of the important factors, introducing the coupling frequency disturbance component. It will further deepen the degree of frequency coupling effect [15]-[16], so it is necessary to consider the influence of asymmetric outer loop control. In [17], the multi-harmonic linearization method

This work was supported by the State Grid Corporation of China (Project name: Stability analysis and control strategy of offshore wind power system considering multi frequency coupling and receiving end grid characteristics; Project number: SGZJ0000KXJS1900419).

was adopted to establish the DC side impedance model of MMC, but the outer loop only considered DC voltage control, and the influence brought by PLL was also ignored. Based on the above situation, it is necessary to establish a more accurate MMC small signal impedance model considering complete control structure.

To solve the above problems, this paper proposes a small signal impedance modeling method of MMC based on multi-harmonic linearization. The impedance model established takes into account the interaction between multiple harmonics in MMC and the complete control structure, and the model has high accuracy. Firstly, on the basis of MMC average mathematical model, the causes and distribution of high order harmonics of various variables in MMC converter are analyzed. Then based on the principle of multi-harmonic linearization, the small signal impedance model of MMC is derived. The model considers the interaction between small signal harmonics and steady-state harmonics and it has high accuracy. Finally, simulation verification is carried out in PSCAD/EMTDC to verified the accuracy of the established model, and the influence of different control mode on the impedance characteristics of MMC is analyzed, which provides a theoretical basis for the stability research of flexible DC power grid.

II. MATHEMATICAL MODEL AND INTERNAL HARMONIC CHARACTERISTICS OF MMC

A. Mathematical model of MMC

Fig. 1 shows the topological structure of the three-phase MMC converter, which is composed of six arms. The upper and lower arms together represent one phase. Each arm is composed of the same N submodules connected in series with the arm reactor. Each submodule can run in the input, cut out and locked states respectively according to the IGBT on/off state. The capacitance of the submodule is denoted by C_{SM}. Because the structure of the three-phase arm is exactly the same, the basic principle of the three-phase MMC can be analyzed by using the single-phase MMC. Taking phase A as an example, the electrical quantities in the figure are: v_{ua} and v_{la} represent the sum of capacitor voltages of submodules of upper and lower arms; i_{ua} and i_{la} represent current of upper and lower arms; U_{dc} and u_{va} represent DC bus voltage and phase voltage at the AC port; I_{dc} and i_{sa} represent DC bus current and phase current at the AC port.

Assuming that there is no difference in the parameters of each submodule, it can be considered that its dynamic characteristics are completely the same, which can be represented by a controlled voltage source. In this case, it can be represented by MMC average mathematical model, and its equivalent circuit is shown in Fig. 2. Using the average mathematical model can eliminate the switching operation and make the discrete bridge arm model continuous. Taking the upper bridge arm of phase A as an example, the following equation can be obtained according to Kirchhoff voltage equation and current equation

Fig. 1. Circuit diagram of MMC converter.

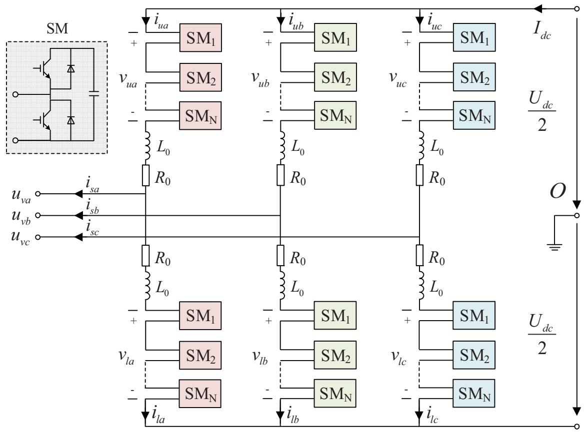

Fig. 2. Equivalent circuit of MMC converter.

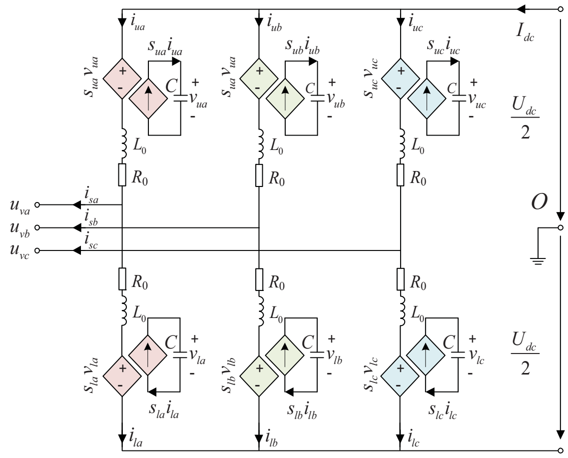

$$L_0 \frac{di_{ua}}{dt} + R_0 i_{ua} = \frac{U_{dc}}{2} - u_{va} - s_{ua} v_{ua} \tag{1}$$

$$C \frac{dv_{ua}}{dt} = s_{ua} i_{ua} \tag{2}$$

where R_0 is the equivalent resistance of the arm, s_{ua} is the switching coefficient of the arm submodules, which is defined as the ratio of the number of submodules in the input to the total number of submodules of the arm, C is the equivalent capacitance of the arm, and its relationship with the capacitance of the submodule is

$$C = \frac{C_{sm}}{N} \tag{3}$$

B. Internal harmonic characteristics of MMC

According to equations (1) and (2), the mathematical model describing the dynamic characteristics of MMC is nonlinear, including the product term of sub-module switching coefficient, which makes MMC different from traditional two-level VSC, and each electrical volume contains multiple harmonics. The reasons are as follows: In equation (1), the product term of the switching coefficient of the arm submodules and the equivalent capacitance voltage of the arm will act on the arm current to generate higher harmonics, while in equation (2), the product term of the switching coefficient of the arm submodules and the bridge arm current will act on the equivalent capacitance voltage of the bridge arm to generate higher harmonics, and its higher harmonic component will continue to act on the bridge arm current to generate higher harmonics. The continuous interaction, the cycle goes on, the arm current and capacitor voltage will produce infinite harmonics. However, due to the filtering effect of the submodule capacitance and the arm reactor, the amplitude of the high harmonics will decrease continuously, and the arm current and submodule capacitance voltage are mainly double frequency. The port impedance characteristics of MMC are closely related to the internal harmonic characteristics, so the influence of multiple harmonics on model accuracy must be considered in modeling.

In the steady-state operation of MMC, the internal harmonic characteristics of MMC is shown in Table I and II. According to Table I and II, the phase sequence between harmonics refers to the characteristic of each electrical parameter between three phases, and the phase relationship between harmonics refers to the characteristic of each electrical parameter between upper and lower bridge arms. In addition, the phase relationship of the current of the arm shows that when the harmonic components of the current in the upper and lower arms are in the same phase, the circulating current will be formed, and the harmonic components are called common mode components. When the harmonic components of the current in the upper and lower arms are in opposite phases, the output current is formed, and the even harmonic components are called differential mode components. In steady-state operation, the electrical design of six arms of MMC is exactly the same, and its internal high order harmonics satisfy symmetry, which greatly simplifies the converter model. Impedance modeling can only be carried out on a single arm, and the state quantities of other arms can be obtained by the symmetric transformation of the arm. In order to simplify the subsequent process, the second subscript in each electrical parameter is deleted below, and no distinction is made.

TABLE I. PHASE SEQUENCE CLASSIFICATION OF INTERNAL HARMONIC OF MMC

Phase Sequence	Harmonic Frequency
Positive sequence	$(3k+1)f_1$
Negative sequence	$(3k-1)f_1$
Zero sequence	$3kf_1$

k=0,1,2,…

TABLE II. PHASE RELATIONSHIP CLASSIFICATION OF INTERNAL HARMONIC OF MMC

Phase Sequence	Harmonic Frequency
Circulation component	$2kf_1$
Output component	$(2k+1)f_1$

k=0,1,2,…

III. MODEL OF MMC MAIN CIRCUIT

By fourier transform, any periodic signal $x(t)$ can be decomposed into DC component and numerous sinusoidal signals of different frequencies, which can be transformed into vector form by euler formula

$$x(t)=\frac{1}{2}\left[X_n e^{-ja_n}\ \cdots\ X_1 e^{-ja_1}\ 2X_0\ X_1 e^{ja_1}\ \cdots\ X_n e^{ja_n}\right]^{\mathrm{T}} \quad (4)$$

Each element corresponds to the harmonic component of frequency $-nf_1,\ \cdots,\ -f_1,\ 0, f_1,\ \cdots,\ nf_1$, and the fundamental frequency is f_1. Using this method, the arm current, the equivalent capacitance voltage of the arm and the switching coefficient of the arm submodules in the time domain can be respectively converted to the frequency domain

$$\boldsymbol{i}_u=\begin{bmatrix} I_n e^{-j\alpha_n} \\ \vdots \\ I_1 e^{-j\alpha_1} \\ I_0 \\ I_1 e^{j\alpha_1} \\ \vdots \\ I_n e^{j\alpha_n} \end{bmatrix}, \boldsymbol{v}_u=\begin{bmatrix} V_n e^{-j\beta_n} \\ \vdots \\ V_1 e^{-j\beta_1} \\ V_0 \\ V_1 e^{j\beta_1} \\ \vdots \\ V_n e^{j\beta_n} \end{bmatrix}, \boldsymbol{s}_u=\begin{bmatrix} S_n e^{-j\gamma_n} \\ \vdots \\ S_1 e^{-j\gamma_1} \\ S_0 \\ S_1 e^{j\gamma_1} \\ \vdots \\ S_n e^{j\gamma_n} \end{bmatrix} \quad (5)$$

where I_n, V_n, S_n, a_n, β_n and γ_n respectively represent the amplitude and phase of the n-th harmonic component of the arm current, the equivalent capacitance voltage of the arm, and the switching coefficient of the arm submodules.

Substituting equation (5) into (1) and (2), convolution operation in the frequency domain is used to replace product operation in the time domain, and the MMC model in the time domain is converted to the frequency domain

$$\boldsymbol{i}_u=\boldsymbol{Y}_L\left(\boldsymbol{V}_{dc}-\boldsymbol{u}_v-\boldsymbol{s}_u\otimes\boldsymbol{v}_u\right) \quad (6)$$

$$\boldsymbol{v}_u=\boldsymbol{Z}_C\boldsymbol{s}_u\otimes\boldsymbol{i}_u \quad (7)$$

where $\boldsymbol{V}_{dc}=\frac{1}{2}[0\ \cdots\ U_{dc}\ \cdots\ 0]^{\mathrm{T}}$, and $\boldsymbol{Y}_L$ is the admittance of the reactance and equivalent resistance of the arm, and $\boldsymbol{Z}_C$ is the impedance of equivalent capacitance of the arm

$$\begin{cases}\boldsymbol{Y}_L=diag\left\{1/\left(R_0+j2\pi nf_1L_0\right)\right\} \\ \boldsymbol{Z}_C=diag\left\{1/\left(j2\pi nf_1C_0\right)\right\}\end{cases} \quad (8)$$

For the convenience of algebra operation, Toeplitz matrix can be used to transform the complicated vector convolution operation into the dot product operation between matrix and vector. Take the $\boldsymbol{s}_u$ as an example, and its Toeplitz matrix is

$$\boldsymbol{S}_u=\begin{bmatrix} \ddots & \cdots & \cdots & \cdots & \iddots \\ \cdots & S_0 & S_1e^{-j\gamma_1} & S_2e^{-j\gamma_2} & \cdots \\ \cdots & S_1e^{j\gamma_1} & S_0 & S_1e^{-j\gamma_1} & \cdots \\ \cdots & S_2e^{j\gamma_2} & S_1e^{j\gamma_1} & S_0 & \cdots \\ \iddots & \cdots & \cdots & \cdots & \ddots \end{bmatrix} \quad (9)$$

After eliminating the convolution operation, the steady-state model of MMC can be expressed as

$$\boldsymbol{i}_u = \boldsymbol{Y}_L\left(\boldsymbol{V}_{dc} - \boldsymbol{u}_v - \boldsymbol{S}_u \boldsymbol{v}_u\right) \tag{10}$$

$$\boldsymbol{v}_u = \boldsymbol{Z}_C \boldsymbol{S}_u \boldsymbol{i}_u \tag{11}$$

The impedance modeling of MMC is carried out by using harmonic linearization method. Taking the AC side as an example, it is assumed that the small voltage disturbance signal $\hat{\boldsymbol{v}}_s$ of frequency f_s is injected at the point of common coupling (PCC) to obtain the current response signal of the same frequency, so as to obtain the AC impedance of MMC. Due to the action of the control loop, the current of the arm, the equivalent capacitance voltage of the arm and the switching coefficient of the arm submodules will all produce the small signal disturbance of frequency $f_s \pm kf_1$, which can be expressed as

$$\hat{\boldsymbol{i}}_u = \begin{bmatrix} \hat{I}_n e^{j\hat{\alpha}_{s-n}} \\ \vdots \\ \hat{I}_1 e^{j\hat{\alpha}_{s-1}} \\ \hat{I}_s e^{j\hat{\alpha}_s} \\ \hat{I}_1 e^{j\hat{\alpha}_{s+1}} \\ \vdots \\ \hat{I}_n e^{j\hat{\alpha}_{s+n}} \end{bmatrix}, \hat{\boldsymbol{v}}_u = \begin{bmatrix} \hat{V}_n e^{j\hat{\beta}_{s-n}} \\ \vdots \\ \hat{V}_1 e^{j\hat{\beta}_{s-1}} \\ \hat{V}_s e^{j\hat{\beta}_s} \\ \hat{V}_1 e^{j\hat{\beta}_{s+1}} \\ \vdots \\ \hat{V}_n e^{j\hat{\beta}_{s+n}} \end{bmatrix}, \hat{\boldsymbol{s}}_u = \begin{bmatrix} \hat{S}_n e^{j\hat{\gamma}_{s-n}} \\ \vdots \\ \hat{S}_1 e^{j\hat{\gamma}_{s-1}} \\ \hat{S}_s e^{j\hat{\gamma}_s} \\ \hat{S}_1 e^{j\hat{\gamma}_{s+1}} \\ \vdots \\ \hat{S}_n e^{j\hat{\gamma}_{s+n}} \end{bmatrix} \tag{12}$$

Linearization of (10) and (11) at the steady-state operating point can be written as

$$\hat{\boldsymbol{i}}_u = -\boldsymbol{Y}_{Ls}\left(\hat{\boldsymbol{v}}_s + \boldsymbol{V}_u \hat{\boldsymbol{s}}_u + \boldsymbol{S}_u \hat{\boldsymbol{v}}_u\right) \tag{13}$$

$$\hat{\boldsymbol{v}}_u = \boldsymbol{Z}_{Cs}\left(\boldsymbol{I}_u \hat{\boldsymbol{s}}_u + \boldsymbol{S}_u \hat{\boldsymbol{i}}_u\right) \tag{14}$$

where $\hat{\boldsymbol{v}}_s = [0 \cdots 0 \;\; \hat{V}_s e^{j\varphi_s} \;\; 0 \cdots 0]^{\mathrm{T}}$, and $\boldsymbol{I}_u$, $\boldsymbol{V}_u$ and $\boldsymbol{S}_u$ are the Toeplitz matrix corresponding to the arm current, the equivalent capacitance voltage of the arm and the switching coefficient of the arm submodules respectively. In addition, due to the change of harmonic characteristics after the injection of disturbance signal, the admittance matrix of the reactance and equivalent resistance of the arm and the impedance matrix of the equivalent capacitance of the arm can be expressed as

$$\begin{cases} \boldsymbol{Y}_{Ls} = diag\left\{1/\left(R_0 + j2\pi\left(f_s + nf_1\right)L_0\right)\right\} \\ \boldsymbol{Z}_{Cs} = diag\left\{1/\left(j2\pi\left(f_s + nf_1\right)C_0\right)\right\} \end{cases} \tag{15}$$

By combining (13) and (14), we can obtain the AC side admittance matrix of MMC

$$\boldsymbol{Y}_{ac} = -\hat{\boldsymbol{i}}_u / \hat{\boldsymbol{v}}_s \tag{16}$$

Thus the AC side impedance of MMC can be obtained from the central element of $\boldsymbol{Y}_{ac}$. In order to eliminate $\hat{\boldsymbol{s}}_u$, it is necessary to obtain the small signal model of MMC control system.

IV. Model of MMC Control Sysytem

Fig. 3. Block diagram of MMC control system.

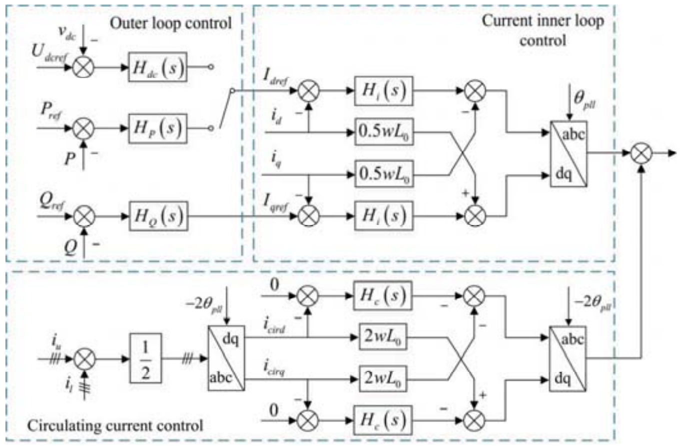

The block diagram of MMC is shown in Fig. 3. To obtain the small signal model of the arm submodules switching coefficient, each control link needs to be modeled respectively. It is assumed that MMC adopts active power control and reactive power control, $\hat{\boldsymbol{s}}_u$ can be expressed as:

$$\hat{\boldsymbol{s}}_u = \boldsymbol{G}_i \hat{\boldsymbol{i}}_u + \boldsymbol{G}_{cir} \hat{\boldsymbol{i}}_u + \boldsymbol{G}_{OP} \hat{\boldsymbol{P}} + \boldsymbol{G}_{OQ} \hat{\boldsymbol{Q}} + \boldsymbol{G}_{pll} \hat{\boldsymbol{v}}_s \tag{17}$$

The control system of MMC is mostly based on synchronous rotating coordinate system. According to Park transformation, the frequency difference between stationary coordinate system and synchronous rotating coordinate system is f_1.When an ideal PLL is used, Park transformation will shift the positive disturbance signal of frequency $f_s + kf_1$ downward f_1, and the negative disturbance signal upward f_1. Also, negative Park transformation of double frequency will shift the positive disturbance signal of frequency $f_s + kf_1$ upward $2f_1$, and the negative disturbance signal downward $2f_1$.

A. Current inner loop and Circulating current control

Since the AC side current is the difference between the current of the upper and lower arms, so only the positive or negative output component of the arm current needs to be considered. According to the block diagram of the current loop control and the above analysis, $\boldsymbol{G}_i$ can be expressed as

$$\begin{cases} \boldsymbol{G}_i = diag\left\{\left|A_k B_k\right|\left[H_i\left(2\pi\left(f_s + kf_1 - B_k f_1\right)\right) - jB_k \pi f_1 L_0\right]\right\} \\ H_i(s) = K_{ip} + \dfrac{K_{ii}}{s} \end{cases} \tag{18}$$

where K_{ip} and K_{ii} are proportional and integral coefficient of current inner loop PI controller. A_k and B_k are defined as

$$A_k = \begin{cases} 1 & k = 2i \\ 0 & k = 2i+1 \end{cases}, \quad B_k = \begin{cases} 1 & k = 3i \\ -1 & k = 3i+1 \\ 0 & k = 3i-1 \end{cases}, i \in Z$$

Similarly, the control goal of the circulating current control is to eliminate the circulation component in the arm current, so only the positive or negative circulation component in the arm current needs to be considered. According to the control block diagram of the circulating current control and the above analysis, $\boldsymbol{G}_{cir}$ can be expressed as

$$\begin{cases} \boldsymbol{G}_{cir} = diag\left\{ \left| \overline{A_k} B_k \right| \left[H_c\left(2\pi\left(f_s + kf_1 + 2B_k f_1\right)\right) + jB_k 4\pi f_1 L_0 \right] \right\} \\ H_c(s) = K_{cirp} + \dfrac{K_{ciri}}{s} \end{cases} \tag{19}$$

where K_{cirp} and K_{ciri} are proportional and integral coefficient of circulating current control PI controller, and $\overline{A_k} = 1 - A_k$.

B. DC voltage outer loop control

According to the block diagram of DC voltage outer loop control, it only works on d-axis, and the control is asymmetric. It is assumed that there is a disturbance signal of frequency of f_s on d-axis, and it can be obtained as

$$x_{abc} = T_{dq-abc} x_d e^{jw_s} = 0.5\left(x_d e^{j(w_s + w_1)} + x_d e^{j(w_s - w_1)}\right) \tag{20}$$

where

$$T_{dq/abc}(\theta) = \begin{bmatrix} \cos\theta & \cos\left(\theta - \frac{2\pi}{3}\right) & \cos\left(\theta + \frac{2\pi}{3}\right) \\ -\sin\theta & -\sin\left(\theta - \frac{2\pi}{3}\right) & -\sin\left(\theta + \frac{2\pi}{3}\right) \end{bmatrix}^T$$

It can be found that two new disturbance signals are generated after Park inverse transformation, the amplitude is half of the original, and the frequency difference is $2f_1$. The DC side equivalent circuit of MMC can be represented by the current source equivalent circuit of Norton form, and only the zero-sequence circulation component in the arm current will flow through the equivalent impedance of the DC side. According to the block diagram of the DC voltage outer loop control and the above analysis, $\boldsymbol{G}_{Vdc}$ is the control function of DC voltage outer loop control on the disturbance signal of arm current and which can be expressed as

$$\begin{cases} \boldsymbol{G}_{Vdc} = -3\boldsymbol{G}_{dc}\boldsymbol{G}_{ir}\boldsymbol{Z}_{dcs} \\ \boldsymbol{G}_{ir} = diag\left\{ \overline{A_k}\,\overline{B_k} H_i\left(2\pi\left(f_s + kf_1\right)\right) \right\} \\ \boldsymbol{G}_{dc} = \dfrac{1}{2}\begin{bmatrix} 0 & \cdots & 0 & 0 & 0 & \cdots & 0 \\ \vdots & \ddots & H_{dc,-1} & \cdots & \cdots & \iddots & \vdots \\ 0 & \cdots & 0 & 0 & 0 & \cdots & 0 \\ 0 & \cdots & H_{dc,-1} & 0 & 0 & \cdots & 0 \\ 0 & \cdots & 0 & 0 & 0 & \cdots & 0 \\ \vdots & \iddots & \cdots & \cdots & \cdots & \ddots & \vdots \\ 0 & \cdots & 0 & 0 & 0 & \cdots & 0 \end{bmatrix} \\ H_{dc}(s) = K_{dcp} + \dfrac{K_{dci}}{s} \end{cases} \tag{21}$$

where $\boldsymbol{Z}_{dcs}$ is the equivalent impedance of the DC side of the MMC after injection of voltage disturbance signal, K_{cirp} and K_{ciri} are proportional and integral coefficient of DC voltage control PI controller, and $\overline{B_k} = 1 - |B_k|$.

C. Power outer loop control

Assuming that MMC adopts active power control, when an ideal PLL is adopted, it can be considered that $V_q = 0$ in the steady state, then after the voltage disturbance signal is injected at PCC point, the active power disturbance signal can be expressed as

$$\hat{P} = \frac{3}{2}\left(V_d \hat{i}_d + I_d \hat{v}_d + I_q \hat{v}_q\right) \tag{22}$$

And then we convert it to the frequency domain

$$\hat{\boldsymbol{P}} = \overline{A_k}\,\overline{B_k}\left(V_P \hat{\boldsymbol{i}}_u + I_P \hat{\boldsymbol{v}}_e\right) \tag{23}$$

where $\hat{\boldsymbol{v}}_e$ is a unit column vector and

$$\begin{cases} V_P = 3V_d\left(I_{-2}e^{-j\alpha_2} + I_0\right) / \left(I_{-1}e^{-j\alpha_1}\right) \\ I_P = 6V_s I_1 \end{cases}$$

According to the block diagram of the active power outer loop control and the above analysis, $\boldsymbol{G}_{OP}$ can be expressed as

$$\begin{cases} \boldsymbol{G}_{OP} = \boldsymbol{G}_P\boldsymbol{G}_{ir} \\ \boldsymbol{G}_P = \dfrac{1}{2}\begin{bmatrix} 0 & \cdots & 0 & 0 & 0 & \cdots & 0 \\ \vdots & \ddots & H_{P,-1} & \cdots & \cdots & \iddots & \vdots \\ 0 & \cdots & 0 & 0 & 0 & \cdots & 0 \\ 0 & \cdots & H_{P,-1} & 0 & 0 & \cdots & 0 \\ 0 & \cdots & 0 & 0 & 0 & \cdots & 0 \\ \vdots & \iddots & \cdots & \cdots & \cdots & \ddots & \vdots \\ 0 & \cdots & 0 & 0 & 0 & \cdots & 0 \end{bmatrix} \\ H_P(s) = K_{Pp} + \dfrac{K_{Pi}}{s} \end{cases} \tag{24}$$

where K_{Pp} and K_{Pi} are proportional and integral coefficient of active power control PI controller.

D. PLL

According to the structure of PLL, the relationship between the output phase angle deviation and the voltage disturbance signal can be obtained

$$\begin{cases} \boldsymbol{\Delta\theta} = F_{pll,-1}\hat{\boldsymbol{v}}_s = \dfrac{-jH_{pll}\left(2\pi\left(f_s - f_1\right)\right)}{1 + V_1 H_{pll}\left(2\pi\left(f_s - f_1\right)\right)}\hat{\boldsymbol{v}}_s \\ H_{pll}(s) = \left(K_{pllp} + \dfrac{K_{plli}}{s}\right)\dfrac{1}{s} \end{cases} \tag{25}$$

where F_{pll} is the closed loop transfer function of PLL, K_{pllp} and K_{plli} are proportional and integral coefficient of PLL.

Under the influence of $\boldsymbol{\Delta\theta}$, Park transformation of the current inner loop control and negative Park transformation of double frequency of the circulating current control will generate the disturbance component.

According to the above analysis, $\boldsymbol{G}_{pll}$ can be expressed as

$$\boldsymbol{G}_{pll}=\begin{bmatrix} 0 & \cdots & 0 & 0 & 0 & 0 & 0 & \cdots & 0 \\ \vdots & \ddots & \cdots & \cdots & g_{pll,-3} & \cdots & \cdots & \iddots & \vdots \\ 0 & \cdots & 0 & 0 & g_{pll,-2} & 0 & 0 & \cdots & 0 \\ 0 & \cdots & 0 & 0 & 0 & 0 & 0 & \cdots & 0 \\ 0 & \cdots & 0 & 0 & g_{pll,0} & 0 & 0 & \cdots & 0 \\ 0 & \cdots & 0 & 0 & g_{pll,1} & 0 & 0 & \cdots & 0 \\ 0 & \cdots & 0 & 0 & 0 & 0 & 0 & \cdots & 0 \\ \vdots & \iddots & \cdots & \cdots & \cdots & \cdots & \cdots & \ddots & \vdots \\ 0 & \cdots & 0 & 0 & 0 & 0 & 0 & \cdots & 0 \end{bmatrix} \quad (26)$$

where

$$\begin{cases} g_{pll,-3}=-jF_{pll,-1}M_{u,2} \\ g_{pll,-2}=-jF_{pll,-1}\left(M_{u,-1}-H_{i,-2}I_{u,-1}\right) \\ g_{pll,0}=jF_{pll,-1}\left(M_{u,1}-H_{i,0}I_{u,1}\right) \\ g_{pll,1}=jF_{pll,-1}M_{u,-2} \end{cases}$$

V. VALIDATION AND ANALYSIS

In order to verify the effectiveness and accuracy of the impedance calculation method proposed in this paper, the impedance model is verified in PSCAD/EMTDC by offline simulation frequency sweep method. By adding a series of small signal voltage disturbances of different frequencies to the AC side of MMC and measuring the small signal current response of the same frequency generated by the disturbance, the AC side impedance models of MMC at different frequencies are calculated. MMC adopts two different control modes, one is constant active power control and constant reactive power control, the other is constant DC voltage control and constant reactive power control. The main parameters of MMC simulation system are shown in Table III.

TABLE III. PARAMETERS OF SIMULATION SYSTEM

Parameter	Value
Arm Inductance	140mH
Arm Equivalent Resistance	0.4Ω
Modules per Arm	400
Module Capacitance	8mF
DC Voltage	500kV
AC L-L Voltage (RMS)	525kV
DC Volatge PI Controller	5+25/s
Active Power PI Controller	0.02+20/s
Reactive Power PI Controller	0.02+20/s
Current Inner Loop PI Controller	1+30/s
Circulating Current PI Controller	0.8+100/s
PLL Controller	(50+100/s)/s

Fig. 4. AC side impedance of MMC.

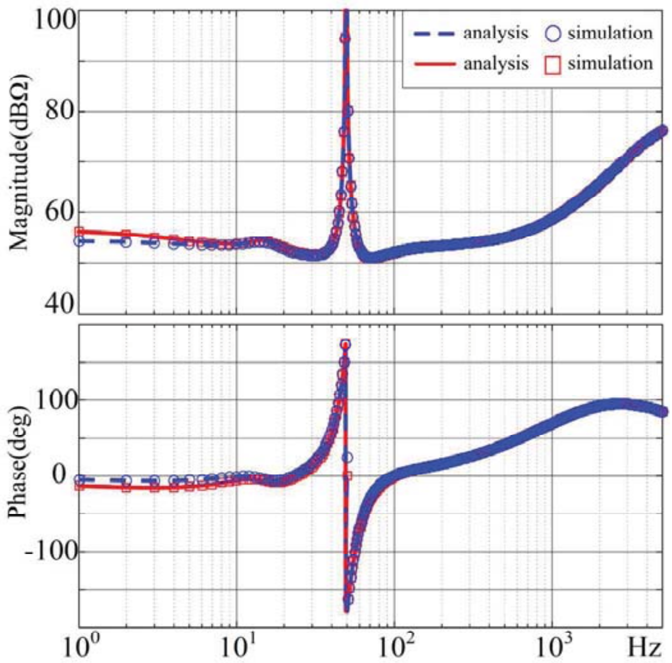

Fig. 4 shows the AC side impedance characteristics of MMC under two control modes respectively. Impedance calculation results of MMC under constant active power control and constant reactive power control are shown in blue dotted lines and its simulation frequency sweep results are shown in blue dots. Impedance calculation results of MMC under constant DC voltage control and constant reactive power control are shown in red solid lines and its simulation frequency sweep results are shown in red squares.

Fig. 4 shows that the method proposed in this paper can accurately calculate the AC side impedance of MMC, and the simulation result almost coincides with the analytical calculation result. When MMC adopts different outer loop control modes, the low frequency band of AC side impedance of MMC will be affected and it also confirms the necessity of modeling different outer loop control modes of MMC.

VI. SUMMARY

In this paper, a small signal impedance modeling method of MMC considering the interaction between internal multiple harmonics and the complete control structure including inner and outer loop control, circulating current control and PLL based on multi-harmonic linearization is proposed. The following conclusions are obtained:

1) The proposed method is verified in PSCAD/EMTDC by offline simulation frequency sweep method and the impedance model is highly accurate. The low frequency band of AC side impedance of MMC is affected under different outer loop control modes.

2) The proposed method provides a theoretical basis for the stability research of flexible DC power grid and it can be extended to different MMC impedance model under various control modes.

References

[1] TANG Guangfu, LUO Xiang, and WEI Xiaoguang, "Multi-terminal HVDC and DC-grid technology," Proceedings of the CSEE, 2013, vol. 33, no. 10, pp. 8-17.

[2] MAJID M, EDRIS P, and SASAN Z, "Dynamic model, control and stability analysis of MMC in HVDC transmission systems," IEEE Transactions on Power Delivery, 2017, vol. 32, no. 3, pp. 1471-1482.

[3] TANG Guangfu, PANG Hui, and HE Zhiyuan, "R&D and Application of Advanced Power Transmission Technology in China," Proceedings of the CSEE, 2016, vol. 36, no. 7, pp. 1760-1771.

[4] YIN Congqi, XIE Xiaorong, LIU Hui, and WANG Xiao, "Analysis and control of the oscillation phenomenon in VSC-HVDC transmission system," Power System Technology, 2018, vol. 42, no. 4, pp. 1117-1123.

[5] SAAD H, FILLION Y, and DESCHANVRES S, "On resonances and harmonics in HVDC-MMC station connected to AC grid," IEEE Transactions on Power Delivery, 2017, vol. 32, no. 3, pp. 1565-1573.

[6] LÜ Jing, DONG Peng, SHI Gang, and CAI Xu, "Subsynchronous oscillation and its mitigation of MMC-based HVDC with large doubly-fed induction generator-based wind farm integration," Proceedings of the CSEE, 2015, vol. 35, no. 19, pp. 4852-4860.

[7] ZOU Changyue, RAO Hong, and XU Shukai, "Analysis of resonance between a VSC-HVDC converter and the AC grid," IEEE Transactions on Power Electronics, 2018, vol. 33, no. 12, pp. 10157-10168.

[8] GUO Xianshan, LIU Zehong, LI Yunfeng, and LU Yajun, "Characteristic analysis of high-frequency resonance of flexible high voltage direct current and research on its damping control strategy," Proceedings of the CSEE, 2020, vol. 40, no. 1, pp. 19-29.

[9] HARNEFORS L, ANTONOPOULOS A, and NORRGA S, "Dynamic analysis of modular multilevel converters," IEEE Trans on Industrial Electronics, 2013, vol. 60, no. 7, pp. 2526-2537.

[10] LIU Huan, YUE Wei, ZHANG Yigong, YI Rong, and ZHANG Haitao, "Circuiting current restraining strategy based on quasi-proportionalresonance control in MMC-HVDC," Automation of Electric Power Systems, 2015, vol. 39, no. 12, pp. 146-151.

[11] SUN Jian, "Impedance-based stability criterion for grid-connected inverters," IEEE Transactions on Power Electronics, 2011, vol. 26, no. 11, pp. 3075-3078.

[12] XUE Yinglin, XU Zheng, ZHANG Zheren, TANG Gen, and XU Feng, "Analysis on converter impedance-frequency characteristics of the MMC-HVDC system," Proceedings of the CSEE, 2014, vol. 34, no. 24, pp. 4040-4048

[13] Lu Jing, Cai Xu, "Harmonic linearization based impedance modeling of modular multilevel converters," Automation of Electric Power Systems, 2017, vol. 41, no. 4, pp. 136-142.

[14] SUN Jian, LIU Hanchao, "Impedance modeling and analysis of modular multilevel converters," Proceedings of the 2016 IEEE 17th Workshop on Control and Modeling for Power Electronics. Trondheim, Norway : IEEE, 2016, pp. 1-9.

[15] LIU Wei, XIE Xiaorong, HUANG Jinkui, ZHANG Chuanyu, and YIN Congqi, "Frequency-coupled impedance model and stability analysis of grid-connected converter," Automation of Electric Power Systems, 2019, vol. 43, no. 3, pp. 138-146.

[16] ZOU Xiaoming, DU Xiong, WANG Guoning, YANG Yougen, and JI Yongliang, "Frequency coupling mechanism analysis and stability judgement for three-phase grid-connected inverter," Automation of Electric Power Systems, 2018, vol. 42, no. 18, pp. 57-63.

[17] XU Dong, WANG Zhang, CHEN Dong, YIN Taiyuan, and YIN Shiyuan, "Modular multilevel converter DC side impedance modeling method considering multi-harmonic coupling of bridge arms," Power System Technology, 2019, vol. 43, no. 7, pp. 2632-2640.